10644–10654 *Nucleic Acids Research, 2014, Vol. 42, No. 16* *Published online 14 August 2014*
doi: 10.1093/nar/gku747

DEAD-box RNA helicase domains exhibit a continuum between complete functional independence and high thermodynamic coupling in nucleotide and RNA duplex recognition

Brighton Samatanga and Dagmar Klostermeier*

Institute for Physical Chemistry, University of Muenster, Correnstrasse 30, 48149 Muenster, Germany

Received June 19, 2014; Revised July 31, 2014; Accepted August 3, 2014

ABSTRACT

DEAD-box helicases catalyze the non-processive unwinding of double-stranded RNA (dsRNA) at the expense of adenosine triphosphate (ATP) hydrolysis. Nucleotide and RNA binding and unwinding are mediated by the RecA domains of the helicase core, but their cooperation in these processes remains poorly understood. We therefore investigated dsRNA and nucleotide binding by the helicase cores and the isolated N- and C-terminal RecA domains (RecA_N, RecA_C) of the DEAD-box proteins Hera and YxiN by steady-state and time-resolved fluorescence methods. Both helicases bind nucleotides predominantly via RecA_N, in agreement with previous studies on Mss116, and with a universal, modular function of RecA_N in nucleotide recognition. In contrast, dsRNA recognition is different: Hera interacts with dsRNA in the absence of nucleotide, involving both RecA domains, whereas for YxiN neither RecA_N nor RecA_C binds dsRNA, and the complete core only interacts with dsRNA after nucleotide has been bound. DEAD-box proteins thus cover a continuum from complete functional independence of their domains, exemplified by Mss116, to various degrees of inter-domain cooperation in dsRNA binding. The different degrees of domain communication and of thermodynamic linkage between dsRNA and nucleotide binding have important implications on the mechanism of dsRNA unwinding, and may help direct RNA helicases to their respective cellular processes.

INTRODUCTION

RNA helicases are found in all kingdoms of life and play a central role in all events of RNA metabolism, including transcription, translation, splicing and structural remodeling (unwinding or annealing of strands). Accordingly, the malfunction of helicases is associated with various pathological disorders such as viral, protozoic, bacterial and fungal infections, neurological disorders and cancer (reviewed in (1)). DEAD-box helicases are the largest group of nucleic acid helicases that unwind double-stranded RNA (dsRNA) in a non-processive reaction utilizing the energy of adenosine triphosphate (ATP) hydrolysis (2). DEAD-box helicases consist of a helicase core that is composed of two flexibly linked domains with structural similarity to the recombination protein RecA (Figure 1A and B). This core is the minimal functional unit of DEAD-box helicases, and contains all ∼13 conserved motifs that are involved in ATP and non-specific RNA binding, as well as coupling of ATP hydrolysis to RNA unwinding (2). In addition to the RecA-like domains of the core, several DEAD-box helicases also possess ancillary N- and C-terminal domains (Figure 1) that are involved in mediating specificity and/or affinity for RNA (3–8) and may contribute to local RNA duplex destabilization (9,10).

During dsRNA unwinding, DEAD-box proteins undergo a series of conformational rearrangements that are linked to their nucleotide cycle (11–13). In the apo-state, the two RecA-like domains (RecA_N, RecA_C) of the helicase core are separated. Cooperative dsRNA and ATP binding induces a large-scale conformational transition to a closed state in which the RecA-like domains are in close proximity (6,11,14–18) (Figure 1B). The closure of the inter-domain cleft locally destabilizes (kinks) the RNA duplex due to steric hindrance with a 'wedge' helix that contains motif Ib, leading to partial separation of the RNA strands (9,10,19,20). An isomerization step results in an intermediate, unwinding-competent complex (21–23). Its formation is accompanied by release of the first RNA strand from the destabilized duplex (24). The structural changes underlying the isomerization reaction have not yet been identified. After release of the first RNA strand, ATP hydrolysis occurs (25). The subsequent release of inorganic phosphate is the rate-limiting step of the nucleotide cycle (18,21,23,26).

*To whom correspondence should be addressed. Tel: +49 251 83 23410; Fax: +49 251 83 29138; Email: dagmar.klostermeier@uni-muenster.de

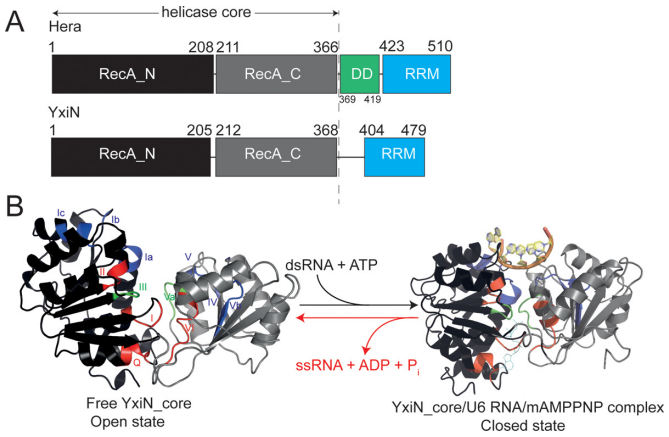

Figure 1. Illustration of motifs and domain structure of Hera and YxiN. **(A)** The N- and C-terminal RecA-like domains are shown in black (RecA_N) and gray (RecA_C), respectively. DD is the dimerization domain and RRM is an ancillary RNA recognition motif. The dotted line indicates the boundary of the helicase cores. **(B)** Homology model of free YxiN_core in the open state (left). Motifs involved in RNA binding are colored blue, and motifs participating in nucleotide binding and hydrolysis are colored red. Green motifs coordinate communication between nucleotide and RNA binding sites. RNA and ATP binding (black arrows) lead to the closed state of the YxiN_core/RNA/nucleotide complex (right). dsRNA unwinding (red arrows) is coupled to ATP hydrolysis causing the release of ADP, ssRNA and inorganic phosphate P_i. The structures of free YxiN_core and YxiN_core/U6 RNA/mAMPPNP complex were modeled by SWISSMODEL using crystal structures of free mjDEAD (PDB: 1hv8) and bound eIF4A-III (PDB: 2hyi) as templates, respectively (12). Structures in (B) were created by PYMOL.

Phosphate dissociation is coupled to re-opening of the core (27). The concomitant disruption of the RNA binding site that is formed by both RecA domains causes dissociation of the second RNA strand. ADP release then regenerates the initial state of the enzyme. The conformational transition from the open to the closed state is necessary for ATPase and dsRNA unwinding activities of DEAD-box helicases (6,28).

In spite of the rather detailed knowledge on the helicase catalytic cycle, the individual roles of the RecA-like domains and their synergy in RNA and nucleotide recognition remain unclear. RNA and nucleotide binding are important steps in the decision on committing the enzyme to the catalytic cycle. A recent study on *Saccharomyces cerevisiae* Mss116 by the Lambowitz group (10) proposed that the RecA_N and RecA_C domains of DEAD-box helicases possess independent modular functions in which RecA_N binds nucleotide and RecA_C binds dsRNA. Based on this conclusion, an unwinding model was suggested in which RecA_C acts as a stationary platform, and unwinding is caused by the incursion of RecA_N (10). To test if these features apply to DEAD-box helicases in general, we investigated the interaction of the isolated RecA_N and RecA_C domains and the helicase cores of the 'heat resistant RNA ATPase' (Hera) from *Thermus thermophilus* ((29), reviewed in (30)) and YxiN from *Bacillus subtilis* (4) with nucleotide and dsRNA by steady-state and time-resolved fluorescence techniques. Our results do not confirm a universal modular function for the RecA-like domains. Instead, we identify the existence of a continuum between complete functional independence and high thermodynamic coupling between the RecA-like domains. Despite their structural similarities and the presence of the same motifs for RNA and nucleotide binding, different helicase cores thus employ different mechanisms of ligand binding. The thermodynamic linkage of RNA and ATP binding seems to be universal across DEAD-box helicases, although the extent of coupling varies. Our results point to fine structural adjustments as a potential important mediator in dsRNA and nucleotide recognition, and suggest the incursion of both RecA-like domains as an alternative pathway to achieve duplex separation. Possibly, the spectrum of binding mechanisms allows different helicases to be regulated differentially or facilitates their targeting to particular biological processes.

MATERIALS AND METHODS

Reagents and RNA preparation

The non-hydrolyzable ATP analog 2′/3′-O-(N-methylanthraniloyl)-adenosine-5′-[(β,γ)-imido] triphosphate (mantAMPPNP) was purchased from Jena Bioscience (Jena, Germany). Polyacrylamide-gel-electrophoresis-purified 14mer self-complementary RNA covalently linked to fluorescein at the 3′-end was purchased from Purimex (Grebenstein, Germany). The RNA sequence is 5′-GGGCGGGCCCGCCC-fluorescein. Double-stranded 14mer RNA (14mer dsRNA) was prepared by incubating the 14mer (142 μM) at 95°C for ∼2.5 min and cooling to room temperature during approximately 1 h. The concentration of 14mer dsRNA was determined by UV absorption after heat denaturation of the duplex (ϵ_{260} = 206 400 M^{-1} cm^{-1}). All experiments were conducted at 25°C in 50 mM Tris-HCl, pH 7.5, 150 mM NaCl, 5 mM $MgCl_2$, 2 mM 2-mercaptoethanol, unless specified otherwise.

Protein production and purification

Hera RecA_N (aa 1–207) and Hera RecA_C (aa 208–369) were produced and purified as Hera_core (aa 1–365) (6). YxiN RecA_N (aa 1–206), YxiN RecA_C (aa 211–370) and YxiN_core (aa 1–368) were produced as glutathion-S-transferase (GST) fusion proteins in *Escherichia coli* Rosetta (DE3) for ∼24 h in auto-inducing medium (31) similar to Hera_core (6). After 5 h at 37°C, the incubation temperature was reduced to 25°C. Purification steps were performed as previously described (14,32). All proteins eluted as monomers from size exclusion chromatography. Crystal structures of Hera RecA_N (33), Hera RecA_C (34) and Hera_core (35) and of YxiN RecA_C (36) indicate that the isolated domains are folded, modular and representative of the intact proteins. In agreement with this modularity, expressed protein ligation of YxiN_1–211-thioester and YxiN_C212–479, produced separately as intein fusions, results in a ligated YxiN with a circular dichroism spectrum and RNA unwinding and ATPase activities similar to the wild-type protein (32). A mixture of YxiN_1–211-*thioester* and YxiN_C212–479 (unligated) cannot hydrolyze ATP or unwind dsRNA (32), underlining the importance of interdomain communication and formation of the closed state for DEAD-box protein activity.

Protein concentrations were determined from the absorption at 280 nm of denatured protein solutions in 6 M GdmCl. The extinction coefficients calculated from the amino acid sequence are Hera RecA_N (11 600 M^{-1} cm^{-1}), Hera RecA_C (7 450 M^{-1} cm^{-1}), Hera_core (18 910 M^{-1} cm^{-1}), YxiN RecA_N (10 810 M^{-1} cm^{-1}), YxiN RecA_C (8 940 M^{-1} cm^{-1}) and YxiN_core (18 490 M^{-1} cm^{-1}) (37).

Fluorescence equilibrium titrations

Steady-state fluorescence (emission and anisotropy) titrations were performed on a Jobin Yvon Fluoromax-3 fluorimeter. K_d values for mAMPPNP complexes in the absence of RNA were determined by titrating RecA_N or core domains with mAMPPNP, and monitoring energy transfer from tryptophans to the mant group. Fluorescence was excited at 280 nm and measured at 444 nm. The fluorescence of free mAMPPNP at 444 nm after direct excitation at 280 nm is negligible. In titrations of nucleotide with the RecA_C domains that lack tryptophan residues, mant fluorescence intensity was used as a probe, with direct excitation at 365 nm. To determine K_d values of nucleotide complexes in the presence of RNA, titrations of ~0.4 μM Hera_core or YxiN_core with mAMPPNP were performed in the presence of excess 3.0 μM 14mer dsRNA, using energy transfer from the mant group to fluorescein as a probe (excitation at 365 nm, emission at 520 nm). The equilibration time in all nucleotide titration experiments was 2–3 min.

To determine K_d values of RNA complexes, 5–50 nM 14mer dsRNA was pre-incubated for 1 h with different concentrations of Hera and YxiN domains. The equilibration time in the presence of 1 mM mAMPPNP was at least 15 min. Fluorescence emission intensity or anisotropy of the fluorescein-labeled RNA was then monitored at 520 nm upon excitation at 496 nm.

Dissociation constants were determined by fitting a 1:1 binding model to fluorescence emission data by non-linear regression in accordance with Equation (1):

$$F = F_o + \Delta F \cdot \frac{(E_{tot} + K_d + L_{tot}) - \sqrt{(E_{tot} + K_d + L_{tot})^2 - (4 \cdot E_{tot} \cdot L_{tot})}}{2L_{tot}} \quad (1)$$

where F is the fluorescence emission, F_o is the fluorescence of free ligand (initial fluorescence), ΔF is the amplitude, E_{tot} is the total concentration of enzyme, K_d is the dissociation constant and L_{tot} is the total ligand concentration. Anisotropy data were analyzed for K_d values by the same 1:1 binding model but accounting for changes in quantum yield of the dye upon complex formation (Equation 2).

$$r = r_f + \frac{[PL] \cdot R}{[PL] \cdot R + L_{tot} - [PL]}(r_B - r_f) \quad (2)$$

$$[PL] = 0.5 \cdot (E_{tot} + K_d + L_{tot}) - \sqrt{(E_{tot} + K_d + L_{tot})^2 - (4 \cdot E_{tot} \cdot L_{tot})}$$

Here, r is the total anisotropy, r_f is the anisotropy of free ligand, r_B is the anisotropy of bound ligand, R is the change in the quantum yield of the dye upon complex formation (ratio of fluorescence intensity of bound to free ligand) and [PL] is the concentration of protein/ligand complex formed.

Time-resolved fluorescence measurements

Time-resolved experiments were performed on a FluoTime 300 single-photon counting system (PicoQuant, Berlin, Germany) equipped with a PDL-800 driver and an LDH-P-C-485 pulsed diode laser head emitting at 479.1 nm. The repetition frequency was 20 MHz (500 nM RNA in absence and presence of 10 μM YxiN) or 10 MHz (500 nM RNA with 10 μM Hera). Fluorophore emission was detected at 519.1 nm using a Hamamatsu R3809U-50 MCP-PMT detector under parallel, perpendicular and magic angle (54.7°) emission polarizer orientations. The time resolution of the instrument set-up is approximately 90 ps. The instrument response function (IRF) was determined using 50% (w/v) silica suspended in buffer. Decay curves were deconvoluted with the IRF signals and analyzed using the FluoFit software (Picoquant, Berlin, Germany). The pre-exponential factors of the fits of the decays measured at magic angle polarizer orientation depend on various factors that include concentrations, extinction coefficients, spectral selection of the species and instrument parameters (38), and cannot be interpreted. The intensity-weighted average lifetimes were calculated as previously described (39). Two rotational correlation times were extracted from the parallel and perpendicularly polarized components of the anisotropy decays by global analysis. The steady-state anisotropy was calculated using the FluoFit software as previously described (40). Further data analysis was done using FluoFit or Origin (OriginLab, Massachusetts, USA) software.

RESULTS

Nucleotide binding to individual RecA-like domains and the helicase core

Previous studies and crystal structures provide support for the structural integrity of isolated Hera and YxiN RecA-like domains and helicase cores (32–36). To dissect the contributions of the RecA_N and RecA_C domains of the helicase core to nucleotide binding, we first determined the nucleotide affinity of the individual domains and the helicase cores of YxiN and Hera in the absence of RNA using the non-hydrolyzable ATP analog mant-AMPPNP (mAMPPNP). Previous studies on YxiN and Hera have established that mAMPPNP is a suitable nucleotide analog to study the initial step of nucleotide binding to DEAD-box helicases (6,27,32). For nucleotide binding to the RecA_N subunits and the helicase cores, Förster resonance energy transfer (FRET) between tryptophan and the mant fluorophore was used as a spectroscopic probe. Titration of ~0.8–1.0 μM protein with increasing concentrations of mAMPPNP resulted in an increase in mant fluorescence due to the binding of mAMPPNP to the RecA_N domains and the helicase cores (Figure 2A). The dissociation constants (K_d, ± standard error of the mean) determined from the binding curves are 733 ± 101 μM (Hera RecA_N), 514 ± 62 μM (Hera_core), 571 ± 7 μM (YxiN RecA_N) and 324 ± 87 μM (YxiN_core). The helicase cores thus bind nucleotide only ~1.4–1.7-fold more tightly than the respective

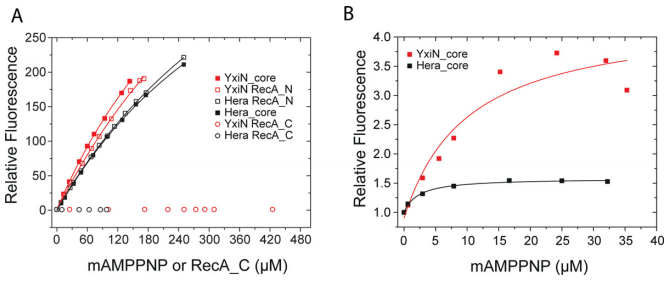

Figure 2. Binding of helicase cores and individual RecA domains to nucleotide in the absence and presence of excess RNA. **(A)** For RecA_N and helicase cores, the relative fluorescence emission at 444 nm after excitation at 280 nm (FRET from Trp to mAMPPNP) was used as a probe to monitor binding. Constant ~0.8–1.0 μM protein was titrated with mAMPPNP. K_d values (± standard error of the mean from two independent experiments) according to analysis with Equation (1) are 733 ± 101 μM (Hera RecA_N), 514 ± 62 μM (Hera_core), 571 ± 7 μM (YxiN RecA_N) and 324 ± 87 μM (YxiN_core). For RecA_C (lacking tryptophans), binding was followed via the fluorescence emission at 444 nm of 1.0 μM mAMPPNP (excitation at 365 nm) with increasing concentration protein. No changes in fluorescence emission are observed. **(B)** Binding of YxiN and Hera cores to nucleotide in the presence of excess RNA, monitored by fluorescence emission at 520 nm upon excitation at 365 nm (FRET from mAMPPNP to the fluorescein coupled to the dsRNA). 400 nM YxiN_core (red) or Hera_core (black) was titrated with mAMPPNP in the presence of saturating 3.0 μM 14mer dsRNA. Data are corrected for background fluorescence of mAMPPNP at 520 nm. The K_d values are 14.8 μM and 2.1 μM for YxiN and Hera_core, respectively. The incubation time was 2–3 min.

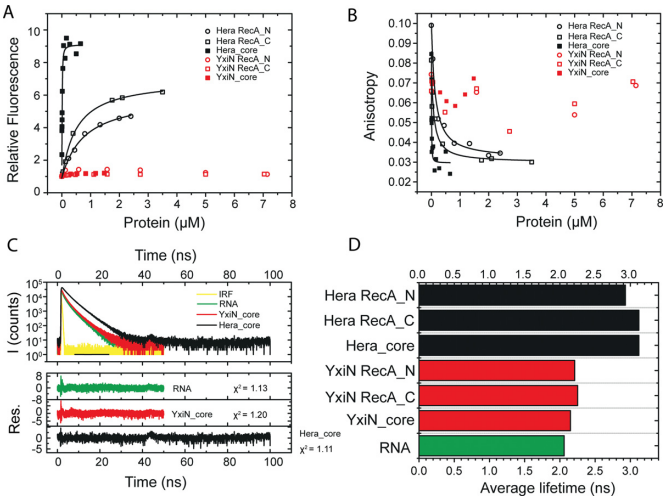

Figure 3. Binding of helicase cores and individual RecA domains to 14mer dsRNA. **(A)** Changes in relative fluorescence emission of 50 nM fluorescein-labeled 14mer dsRNA upon incubation with different concentrations of Hera (black) or YxiN (red). There is no detectable fluorescence change by YxiN_core, RecA_N or RecA_C, indicative of no binding to the 14mer dsRNA. The dissociation constants (K_d) for Hera are 889 ± 236 nM (Hera RecA_N), 327 ± 161 nM (Hera RecA_C) and 7 ± 3 nM (Hera_core). The errors are standard deviations of three independent measurements. **(B)** Fluorescence anisotropy of 50 nM 14mer dsRNA upon incubation with Hera (black) and YxiN (red). Hera binding to dsRNA reduces the anisotropy. Addition of YxiN to the RNA has no effect on the anisotropy. The K_d values for Hera/RNA complexes (three measurements) were similar to those determined in (A). **(C)** Representative time-domain fluorescence intensity decays (I, in photon counts) of 500 nM 14mer dsRNA measured at room temperature with the emission polarizer oriented at 54.7° (magic angle) in the absence (green) and presence of 10 μM Hera_core (black) or YxiN_core (red). Fluorescence decays of the RecA_N and RecA_C subunits were similar to the respective cores (Supplementary Figure S2). Three fluorescence lifetimes (Table 1) were determined from the decays, deconvoluted by the IRF (yellow). **(D)** Intensity-weighted average lifetimes of 14mer dsRNA in the absence (green) and presence of 10 μM Hera (black) or YxiN (red) subunits. All measurements were performed in 50 mM Tris-HCl pH 7.5, 150 mM NaCl, 5 mM $MgCl_2$, 2 mM 2-mercaptoethanol.

isolated RecA_N domains, demonstrating that the thermodynamic contributions of potential contacts with RecA_C are minimal, and the nucleotide is predominantly bound by RecA_N. We next determined the nucleotide affinities of the RecA_C domains in titrations of 1.0 μM mAMPPNP with YxiN_RecA_C and Hera_RecA_C. Due to the lack of tryptophans in RecA_C, mant fluorescence and anisotropy served as spectroscopic probes for binding. Binding of Hera RecA_N to mAMPPNP can be followed by mant fluorescence intensity and anisotropy (Supplementary Figure S1). However, in titrations of nucleotide with RecA_C, neither significant changes in mant fluorescence intensity (Figure 2A) nor in anisotropy (Supplementary Figure S1) were observed. Thus, we conclude that the isolated RecA_C domains of Hera and YxiN do not bind to nucleotide. Altogether, nucleotide binding to the Hera and YxiN helicase cores is therefore similar to the binding mode reported for Mss116 (10), with nucleotide binding by RecA_N, and no significant contributions of RecA_C to binding.

Contributions of RecA_N and RecA_C to RNA binding

To understand the communication between N- and C-terminal RecA-like domains during RNA recognition, we next determined the affinities of the isolated RecA_N and RecA_C and the entire helicase core to a 14mer self-complementary dsRNA labeled with fluorescein at the 3′-end (14mer dsRNA), using fluorescein intensity or anisotropy as a probe. This 14mer dsRNA has previously been used in the structural study of duplex RNA recognition by Mss116 (10). In the absence of nucleotide, we detected no significant changes in fluorescence emission in titrations with YxiN RecA_N or RecA_C, or with the helicase core (Figure 3A), suggesting that YxiN_core does not bind to the 14mer dsRNA in this concentration range. From the concentrations used (50 nM dsRNA, up to 100 μM YxiN_core), we can estimate a lower limit for the K_d of the YxiN_core/RNA complex of approximately 100 μM. To exclude the possibility that the YxiN RecA_N and RecA_C domains bind to RNA without detectable changes in fluorescence emission, we performed steady-state fluorescence anisotropy titrations. Again, there was no significant change in fluorescein anisotropy of the 14mer dsRNA upon incubation with YxiN domains or the entire core, confirming the lack of (high-affinity) binding (Figure 3B).

In contrast to YxiN, the Hera RecA_N and RecA_C domains, as well as the helicase core led to an increase in fluorescence emission as function of Hera concentration, indicative of RNA binding. The crystal structure of the Mss116/RNA complex shows that Mss116 binds one 14mer dsRNA molecule (10), and we therefore analyzed the observed binding curves with a one-to-one binding model according to Equation (1). The dissociation constants (± standard deviation) are 889 ± 236 nM (Hera RecA_N), 327

± 161 nM (Hera RecA_C) and 7 ± 3 nM (Hera_core). Both Hera RecA_N and RecA_C therefore bind to dsRNA individually, with RecA_C showing a slightly (2.7-fold) higher affinity. Hera_core binds the 14mer dsRNA about 127- and 47-fold more tightly than the isolated RecA_N and RecA_C domains, respectively, demonstrating a high level of communication between the individual domains during dsRNA binding.

Anisotropy titrations of the 14mer RNA with Hera RecA_N, RecA_C or Hera_core were in agreement with the binding observed by the increase in fluorescence intensity (Figure 3B). In all cases, protein addition caused a decrease in fluorescence anisotropy with increasing protein concentration. Commonly, binding events lead to an increase in anisotropy due to a slower overall tumbling (increase in rotational correlation time) of the resulting higher molecular weight complex. The anisotropy decrease observed upon Hera binding to the RNA led us to speculate that the rotational correlation time of the Hera/dsRNA complex was much higher than the excited state lifetime of the fluorophore, such that the excited state emission would decay completely before any appreciable depolarization due to rotational tumbling of the complex had occurred.

To confirm that the decrease in steady-state anisotropy reflects binding, we dissected the effect of Hera/dsRNA complex formation on fluorescence lifetimes and rotational correlation times of the fluorescein attached to the RNA by performing time-resolved anisotropy decay experiments with 500 nM 14mer dsRNA in the absence and presence of 10 μM Hera (RecA_N, RecA_C or core). Under these conditions, almost all RNA molecules are bound to protein (100, 96 and 91% to Hera_core, RecA_C and RecA_N, respectively) according to the respective K_d values (Figure 3A). First, we measured the time-domain fluorescence intensity decays under magic angle polarizer orientation so as to acquire data devoid of rotational diffusion and/or anisotropy effects (Figure 3C and Supplementary Figure S2) (41). The intensity decays, deconvoluted with the IRF, were best described by a sum of three exponential functions, yielding three fluorescence lifetimes, τ_1 to τ_3 (Table 1). This model is supported by the non-systematic distribution of the residuals of the fits. Support plane (and Bootstrap) error analyses confirm the significance of the obtained lifetimes (Supplementary Figure S3). Hera/dsRNA complex formation led to a general increase in fluorescence lifetime. In contrast, the lifetime of the fluorescein was identical in the presence and absence of YxiN_core, confirming lack of binding. The molecular origin of the three lifetimes is not clear, as only one RNA species (free or bound) should be populated in all experiments. One possible reason could be related to the fact that each RNA duplex contains two (chemically identical) fluorophores. To simplify comparison, we calculated the intensity-weighted average lifetimes (Figure 3D and Table 1). In contrast to amplitude-weighted average lifetimes, intensity-weighted average lifetimes are much less sensitive to the model used in fitting (39), although both lifetimes show similar trends in our experiments (Supplementary Table S1). The average lifetime of the free dsRNA was ∼2.2 ns (Figure 3D). In the presence of Hera_core, it increased significantly (to ∼3.0 ns), in agreement with the increase in steady-state fluorescence intensity upon complex formation. For YxiN, the absolute and average lifetimes in presence of saturating concentrations of the different constructs were similar to those for unbound RNA (Table 1; Figure 3D), again consistent with YxiN_core not binding the 14mer dsRNA under these conditions.

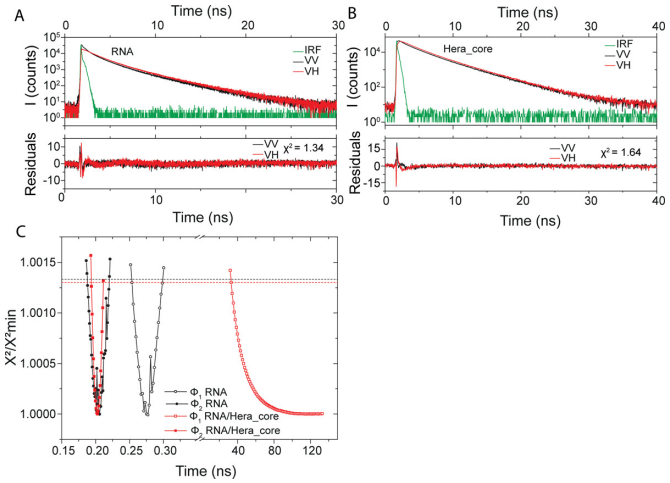

Figure 4. Time-resolved anisotropy decays of fluorescein-labeled 14mer dsRNA in the absence **(A)** and presence of 10 μM Hera_core **(B)**. The parallel (VV, black) and perpendicular (VH, red) anisotropy decays are described by three lifetimes and two rotational correlation times (Table 1). The IRF is shown in green. **(C)** Support plane error analyses of the long (Φ_1 [ns]) and short (Φ_2 [ns]) rotational correlation components of free RNA (black) and Hera_core-dsRNA complex (red). The dotted lines indicate the 75% confidence interval and are colored accordingly.

We then measured the time-domain anisotropy decays of the RNA in the absence and presence of Hera and YxiN domains. Representative anisotropy decays of the 14mer dsRNA in the absence and presence of Hera_core are shown in Figure 4A and B. The fluorescence anisotropy decay of RNA in the presence of YxiN_core is similar to that of free RNA. The decays in the presence of RecA_N and RecA_C domains are similar to those in the presence of the respective cores (Supplementary Figures S4 and S5). Anisotropy decays, deconvoluted with the IRF, were best described by a sum of two exponentials, giving two rotational correlation times, Φ_1 and Φ_2 (Table 1), in addition to the three fluorescence lifetimes (Table 1). Including a third rotational component did not lead to significant improvement of the fit as judged by the χ^2 value. The rotational correlation times of RNA in the absence and presence of YxiN_RecA_N and _RecA_C were similar ($\Phi_1 \sim 0.9$ ns and $\Phi_2 \sim 0.1$ ns). We attribute the smaller rotational correlation time Φ_2 ($\leq$ 0.2 ns) to the segmental flexibility of the attached fluorescein fluorophore, and Φ_1 to the rotational diffusion of the macromolecule. The measured Φ_2 is similar to ∼0.14 ns for fluorescein in water, and the Φ_1 of unbound RNA is similar to that of the fluorescein-labeled 21mer duplex (2.1 ns; (42)), supporting this assignment. Φ_2 in the presence of Hera (∼0.2 ns) is slightly increased, but can still be accounted for by the segmental flexibility of fluorescein. However, Φ_1 is much larger in the presence of Hera than for the free RNA, and ranges from 113 to 13 100 ns (Table 1), consistent with slower rotational diffusion due to complex formation. Support plane analyses with 75% con-

Table 1. Time-resolved parameters describing the association of YxiN or Hera subunits with 14mer dsRNA

	τ_1 (ns)	τ_2 (ns)	τ_3 (ns)	$\bar{\tau}$ (ns)	β_1	Φ_1 (ns)	β_2	Φ_2 (ns)	r_{ss}
RNA only	3.41	1.28	0.14	2.06	0.20	0.86	0.27	0.10	0.095
YxiN_core	3.46	1.32	0.15	2.15	0.16	0.98	0.26	0.13	0.088
YxiN RecA_C	3.55	1.36	0.16	2.25	0.12	0.94	0.28	0.16	0.071
YxiN RecA_N	3.53	1.33	0.15	2.21	0.21	0.69	0.40[a]	0.07	0.090
Hera_core	14.93	3.82	1.83	3.12	0.02	113	0.41	0.21	0.045
Hera RecA_C	12.79	3.79	1.76	3.12	−0.01	13100	0.37	0.24	0.020
Hera RecA_N	13.64	3.72	1.67	2.93	−0.01	1960	0.44	0.21	0.018

τ_1, τ_2 and τ_3 are the fluorescence decay lifetimes; $\bar{\tau}$ is the intensity-weighted average lifetime; β_1 and β_2 reflect the extent of depolarization of the process(es) with rotational correlation times of Φ_1 and Φ_2, respectively; r_{ss} is the calculated steady-state anisotropy. β_2 terms do not exceed 0.4 within error of fit, e.g. β_2 for Hera RecA_N is 0.437 ± 0.032.
[a]β_2 fixed during fit.

fidence established that the rotational correlation times of the Hera/dsRNA complexes exceed 30 ns (Figure 4C). Determination of the rotational tumbling time of the Hera core/dsRNA complexes is thus precluded by the low count rates at such timescales. The rotational correlation time of proteins can be estimated from their molecular weight, the viscosity of the buffer (∼0.089 cP), a typical specific volume for globular proteins of 0.73 ml/g and a protein hydration of 0.23 g water/gram protein using the Perrin equation. The estimated rotational correlation time of free Hera_core (38.7 kDa) is 13.5 ns. The measured Φ_1 of the dsRNA in the presence of Hera_core is larger than this calculated Φ_1 for free Hera_core, further confirming the formation of a Hera_core/dsRNA complex. The estimated rotational correlation time for free YxiN_core ($M_r = 41.6$ kDa) according to the Perrin equation is 14.5 ns. Thus, a similarly high rotational correlation time as observed for Hera would be expected for a YxiN/dsRNA complex, again confirming that neither YxiN RecA_N or RecA_C nor YxiN_core binds to the 14mer dsRNA.

The steady-state anisotropies calculated from the rotational correlation times obtained from anisotropy decays (Figure 4 and Table 1) confirm that Hera binding to RNA does indeed lead to a decrease in the steady-state anisotropy from 0.095 (free dsRNA) to less than 0.045 (bound RNA), in agreement with the steady-state measurements. The anisotropies calculated from rotational correlation times are similar in the absence and presence of YxiN, also consistent with the steady-state anisotropy titrations. The decrease in fluorescein anisotropy upon RNA binding of Hera is explained by analyzing the pre-exponential β_k factors that correspond to each anisotropy decay component with the rotational correlation time Φ_k (Table 1). β_k depends on the excitation and emission dipoles, as well as the rotational diffusion coefficient of the macromolecule (43,44), and varies between −0.2 and 0.4 in one-photon excitation. A non-zero β_k represents the extent to which the emission is depolarized by each rotational component. In contrast, β_k is zero when the fluorescence is not depolarized by the process(es) leading to the anisotropy decay component Φ_k (43). Table 1 shows that β_2 is non-zero and larger than 0.25 in all measurements. β_2 is related to Φ_2, assigned to the segmental mobility of the fluorophore, and its value indicates that the segmental fluorophore mobility contributes to the depolarization of the emission in the absence of Hera or YxiN. For the Hera/dsRNA complexes, β_2 is larger, in agreement with a larger extent of depolarization due to segmental fluorophore mobility. The segmental mobility of fluorescein in the RNA is not reduced by binding to Hera_core or in presence of YxiN_core, indicating that the proteins do not interact with the dye. In free RNA and YxiN/RNA mixtures, β_1 is also large. β_1 is related to Φ_1, assigned to the overall rotational diffusion of the RNA (or the RNA/protein complex). Thus, rotational diffusion of the free dsRNA leads to further depolarization of the emission anisotropy in these cases. However, β_1 is close to zero for Hera/dsRNA complexes (Table 1). This value implies that the rotational diffusion of the Hera/dsRNA complexes does not depolarize the excited state emission. As a consequence, the steady-state anisotropy of Hera/dsRNA complexes is lower than that of free RNA simply because the macromolecular tumbling of Hera/dsRNA complexes occurs on a very different timescale from the excited state emission ($\Phi >> \tau$) and thus does not contribute to depolarization. Similar situations in which the timescale of depolarization due to rotational diffusion exceeds excited state lifetimes have been simulated (43) and have been reported for the binding of methionine tRNA labeled at the 3′-end with fluorescein to methionyl-tRNA synthetase (41,45).

In summary, steady-state and time-resolved fluorescence intensity and anisotropy measurements consistently show that the isolated Hera RecA_N, RecA_C and Hera_core bind dsRNA, whereas the corresponding YxiN domains show no RNA binding in the absence of nucleotide. The dsRNA affinity of YxiN_core is at least two orders of magnitude lower than the dsRNA affinity of Hera_core and of Mss116_core (10,18), clearly setting YxiN_core apart from these DEAD-box helicases.

Thermodynamic coupling of nucleotide and RNA binding to the helicase core

Next, we investigated the influence of nucleotide on the binding of Hera and YxiN cores to 14mer dsRNA. To that end, we titrated 5–50 nM 14mer dsRNA with the helicase cores in the presence of 1 mM mAMPPNP, and measured changes in fluorescence emission of the 14mer dsRNA after direct excitation of fluorescein (Figure 5). The fluorescence intensity significantly increased with increasing concentrations of Hera_core (Figure 5A) or YxiN_core (Figure 5B), indicating that both helicase cores bind the 14mer dsRNA

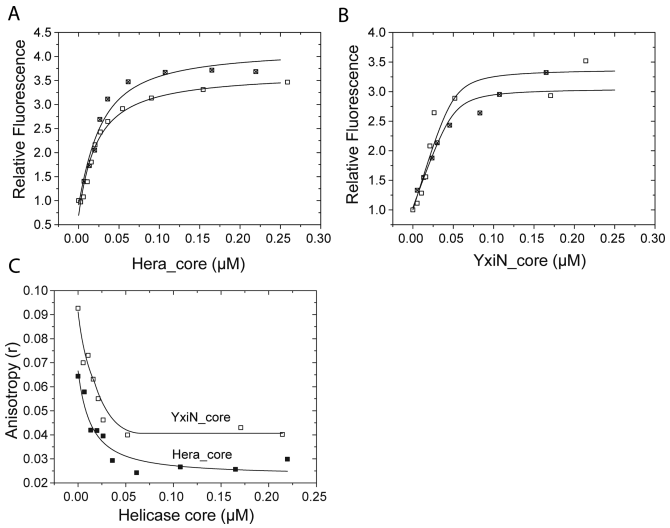

Figure 5. Binding of helicase cores to RNA in the presence of nucleotide. Relative changes in fluorescence emission at 520 nm of 5–50 nM 14mer dsRNA after direct excitation at 496 nm. 14mer dsRNA was titrated with Hera_core **(A)** or YxiN_core **(B)** in the presence of 1.0 mM mAMPPNP (∼70% protein saturation). Data from two independent measurements (open and crossed squares) were analyzed in a global fit according to Equation (1). The K_d values are 15.1 nM and 2 nM for Hera and YxiN_core, respectively. **(C)** Reduction in steady-state fluorescence anisotropy of 14mer dsRNA upon binding of Hera_core (filled squares) or YxiN_core (open squares) to the RNA. The conditions were the same as in (A). The equilibration time was at least 15 min.

tightly when nucleotide is present. The dissociation constants (K_d) determined by global data analysis according to Equation (1) are 2.0 nM and 15.1 nM for the YxiN_core and Hera_core/RNA complexes, respectively. We further confirmed these results by steady-state anisotropy titrations (Figure 5C). The fluorescence anisotropy of the 14mer dsRNA upon addition of Hera_core or YxiN_core decreases as a function of protein concentration, confirming that both helicase cores bind to the RNA when nucleotide is already bound.

To evaluate the reciprocal effect of bound RNA on the nucleotide affinity, we titrated increasing concentrations of mAMPPNP into ∼400 nM Hera_core or YxiN_core in the presence of 3.0 μM 14mer dsRNA, and monitored binding via FRET effect between the mant group and the fluorescein attached to the 14mer dsRNA (Figure 2B). Measured fluorescence intensities were corrected for the contribution of mAMPPNP to the emission at 520 nm (Supplementary Figure S6). The direct excitation of fluorescein at 365 nm is negligible. From the binding curves, we obtain dissociation constants for the mAMPPNP complexes of 2.1 μM and 14.8 μM for Hera_core and YxiN_core, respectively. Thus, prior binding of dsRNA to Hera_core increases the nucleotide affinity 224-fold. The affinity of YxiN_core for nucleotide is 28-fold higher in the presence of dsRNA than in its absence. However, our previous experiments (see above) show that dsRNA is not bound by YxiN_core in the absence of the nucleotide. Therefore, the dissociation constant measured for the YxiN_core/RNA/nucleotide complex is the result of the subsequent processes of nucleotide binding, followed by dsRNA binding to the nucleotide complex. Taken together, Hera_core binds dsRNA and nucleotide in a random process, whereas YxiN_core shows sequential binding, with dsRNA binding to the YxiN/nucleotide complex only. dsRNA and nucleotide binding to the Hera_core and YxiN_core show a strong thermodynamic linkage, but the underlying mechanism for cooperativity between the two RecA domains is different.

DISCUSSION

Nucleotide binding to DEAD-box proteins is mediated by RecA_N

We have shown here that nucleotide binding to the Hera and YxiN helicase cores is mainly mediated by their RecA_N domain, as reported previously for *S. cerevisiae* Mss116 (10). In the structure of the Hera_core/AMP complex, the nucleotide is exclusively contacted by residues from RecA_N (35), supporting our thermodynamic data. The DEAD-box helicase signature motifs involved in ATP binding, namely the Q-motif, and motifs I (Walker A), II (Walker B/DEAD) and III, are all located in the RecA_N domain (Figure 1), in agreement with predominant interactions between nucleotide and the N-terminal domain (reviewed in (46,47)). In structures of the closed conformation of DEAD-box proteins in complex with RNA and nucleotide (20,48), two arginines from motif VI (H**R**IG**R**TGRA), located in RecA_C, contact the γ-phosphate of ATP (49). Mutations of these arginines do not affect the Michaelis constant (K_m) for ATP, but the turnover number for ATP hydrolysis (k_{cat}) is drastically reduced (50). Hence, these interactions seem more important for ATP hydrolysis than for binding itself. The dissociation constants determined for the nucleotide complexes of the Hera and YxiN RecA_N domains and their helicase cores (400–640 μM) we report here are similar to those of other DEAD-box helicase/nucleotide complexes: YxiN-ATP (∼346 μM; (32)), YxiN-AMPPNP (308 μM; (27)) and DbpA-AMPPNP (> 1300 μM; (51)). They are also similar to the K_M values for eIF4A-ATP (440 μM; (15)) and Ded1p-ATP (300 μM; (16)). For DEAD-box proteins, K_M values for ATP should be similar to the K_d value because phosphate release is the rate-limiting step for product formation. Altogether, these results suggest that nucleotide binding predominantly by the N-terminal RecA-like domain is a general feature of DEAD-box proteins.

The individual contributions of the RecA domains to dsRNA binding vary among DEAD-box proteins

In contrast to YxiN, Hera_core as well as the individual Hera RecA_N and RecA_C domains tightly bind to the 14mer dsRNA. These results are in contrast to the previous report that showed dsRNA binding to Mss116_core in the absence of ATP via RecA_C without appreciable participation of the RecA_N domain (10). Our findings demonstrate that dsRNA recognition is not an exclusive function of the C-terminal RecA-like domain, but the N-terminal domain may contribute substantially to binding. The presence of RNA binding motifs in both RecA domains (46) rationalizes the ability of both isolated domains to interact with dsRNA. The higher RNA affinity of the Hera core relative to the isolated domains (47–127-fold) can be explained by

the joint contribution of the RNA binding motifs located in the N- and C-terminal domains to RNA affinity of the Hera core.

In contrast to Hera and Mss116, neither YxiN_core nor the isolated RecA_N or RecA_C domains binds to the 14mer dsRNA in the absence of nucleotide. Although the lack of RNA binding to the YxiN_core was somewhat unexpected, such a situation is not unique. *Mouse* eIF4A (15) and *S. cerevisiae* Ded1 (16) similarly do not bind dsRNA in the absence of nucleotide.

The RNA affinity of Hera RecA_C is only slightly higher than that of the RecA_N (~2.7-fold), suggesting the 14mer dsRNA is most likely already contacted by both domains in the absence of nucleotide. This scenario implies that the RNA substrate could mediate the communication between the RecA_N and RecA_C domains of Hera. Such an RNA-mediated communication is not possible for YxiN, where the core does not bind dsRNA in the absence of nucleotide, or for Mss116, where only RecA_C contributes to dsRNA binding to the core (52). The helicase cores of YxiN, Hera and Mss116 share the same signature motifs and similar structures, and show similar average distances between the RecA domains in the helicase core (6,53,54). Nevertheless, their different behavior with respect to dsRNA binding illustrates that the RNA binding mode and the level of communication between the RecA-like domains of the helicase core in RNA recognition can vary tremendously for different DEAD-box proteins.

Thermodynamic linkage between nucleotide and RNA recognition

YxiN_core does not bind dsRNA in the absence of nucleotide (K_d > 100 μM), but shows tight RNA binding (K_d of ~2 nM) in the nucleotide-bound state. Similar nucleotide-dependent binding has been observed for eIF4A and ssRNA (55). For Hera_core, the presence of nucleotide apparently does not lead to an increase in RNA affinity on the basis of the directly measured affinities. It has to be noted, however, that the experimentally determined value for dissociation of dsRNA from the Hera_core/nucleotide complex (15 nM) has to be regarded as an upper limit. From a thermodynamic perspective, the free energy of forming the ternary complex of the helicase core with nucleotide and dsRNA is independent of the order in which the ligands are bound. In other words, the product of the two equilibrium constants for the two binding events leading to the ternary complex (Figure 6) should be identical within the error of the experiment. Based on these considerations, we can calculate the expected K_d value for dissociation of dsRNA from the Hera_core/nucleotide complex as ~31 pM (Figure 6). There are two possible explanations for the discrepancy between the expected and measured values. First, binding curves (and K_d values) are best defined when ligand concentrations are in the range of the expected dissociation constant. However, an RNA concentration in the pM range is below the detection limit of the fluorescence spectrometer, and the starting RNA concentration of 5–15 nM, above the expected K_d value, might have caused the higher apparent K_d. Second, the 15–30 min incubation time of Hera_core/mAMPPNP complexes with dsRNA during

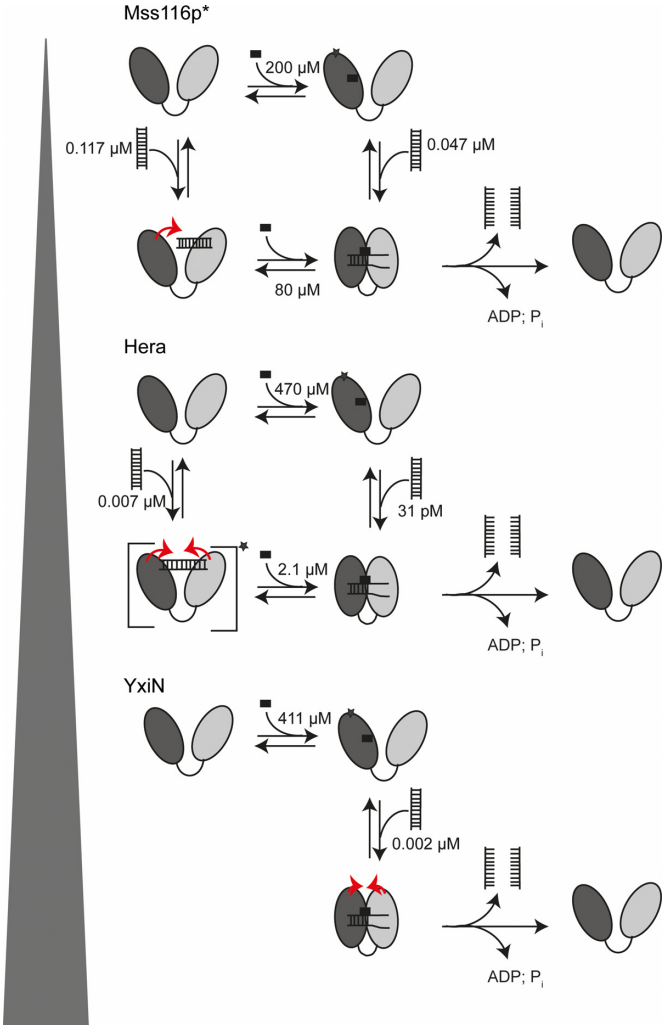

Figure 6. Continuum from complete functional independence of RecA-like domains to high thermodynamic coupling. Summary of nucleotide and dsRNA binding mechanisms for different DEAD-box helicases. The black star denotes an intermediate. Dissociations constants are included. The large arrow head (left, gray) symbolizes increasing thermodynamic coupling from Mss116 through Hera to YxiN. *The model for functional independence of the Mss116p RecA-like domains in nucleotide and RNA binding was derived from (10). The K_d values are from (18). The K_d values for dissociation of RNA from the nucleotide/RNA/complex of Mss116 (18) and Hera_core were calculated from the energetic balance of the thermodynamic cycle.

the titration may not have been sufficient to reach equilibrium at each point in the titration, again leading to a higher apparent K_d value. Because of the thermodynamic considerations outlined above, we can conclude from the increased nucleotide affinity in the presence of RNA (see below) that reciprocally the RNA affinity has to increase in the presence of nucleotide. RNA binding to Hera_core leads to a 250-fold increase in nucleotide affinity (summarized in Figure 6), whereas RNA binding to YxiN_core only increases nucleotide affinity by 28-fold. The K_d value determined from the titration of YxiN_core with nucleotide in the presence of dsRNA does not measure nucleotide binding to an RNA complex, however, because of the sequential binding. YxiN_core first binds nucleotide added in each

titration step and the nucleotide-bound state will then bind the RNA already present. RNA binding is slow and may not reach equilibrium in each titration step, and the K_d value is again upper limit for the true K_d. Hence, the thermodynamic coupling of nucleotide and RNA binding to YxiN may be even higher. The coupling of RNA and ATP binding is lowest for Mss116 (18) (Figure 6).

In conclusion, our results show strong thermodynamic linkage between nucleotide and dsRNA recognition for both Hera and YxiN cores, although possibly to different extents. Overall, the thermodynamic linkage of dsRNA and ATP binding seems to be universal across DEAD-box helicases, but the extent of this energetic coupling differs.

Implications for the mechanism of RNA unwinding by DEAD-box proteins

Our results indicate that nucleotide binding induces conformational changes in DEAD-box proteins that modulate RNA affinity. Indeed, nucleotide-dependent conformational changes in the absence of RNA have been deduced from the Hera RecA_N/AMP crystal structure (33) and from high-field electron-nuclear double resonance spectroscopy of DbpA (56). Conformational changes upon nucleotide binding are mediated by the structural plasticity of both the Q-motif and the P-loop during sensing of the adenine base and the phosphates (33). The requirement for nucleotide binding to YxiN_core (or eIF4A (55)) prior to RNA binding is also consistent with the existence of a nucleotide-bound intermediate that precedes the closed state with both nucleotide and RNA bound (6,14,27).

In contrast to the universal mode of nucleotide binding via RecA_N, dsRNA binding to Hera_core and YxiN_core is different (Figure 6). While both RecA-like domains contribute to dsRNA binding to Hera_core already in the absence of nucleotide, RNA binding to YxiN_core requires prior nucleotide binding. Interestingly, the nucleotide-independent dsRNA binding modes of the Hera, Mss116 and YxiN cores are representative of all three scenarios possible in DEAD-box helicases: either (1) both RecA-like domains tightly bind RNA (Hera), (2) one of the two RecA-like domains tightly binds RNA (Mss116), or (3) none of the two RecA-like domains binds RNA (YxiN). Our results clearly show that the RecA-like domains in DEAD-box proteins can communicate to different extents across these three possibilities. In terms of functional independence of the domains, Mss116 is an extreme case with its independent, modular functions of the two RecA domains in nucleotide (RecA_N) and RNA binding (RecA_C) (10). YxiN seems to represent the opposite end of the spectrum, with nucleotide binding to one domain required for RNA binding to both domains. Our results therefore support the existence of a continuum between complete functional independence and different degrees of thermodynamic coupling between the RecA-like domains (Figure 6). Binding of ATP and RNA leads to the formation of the closed conformation of the helicase core and thus to ATP-dependent RNA unwinding. An overall increased propensity to adopt the closed conformation, brought about by highly coupled ATP and RNA binding, could increase the overall unwinding efficiency. Since phosphate release is the rate-limiting step in the catalytic cycle of DEAD-box proteins, RNA-dependent ATP hydrolysis and duplex unwinding are most likely not affected by the mechanism that led to closing once the closed conformer has been formed. Instead, variations in the interactions with nucleotide and RNA may influence RNA specificity. It has recently been shown that Cyt-19, a general RNA chaperone that is homologous to Mss116, binds to exposed duplexes in non-native intermediates of group I intron RNA (57). Binding to these duplexes and unwinding are modulated by the flexibility of the folding intermediate, and increase with duplex accessibility. It is conceivable that, in addition to the structure and dynamics of the RNA substrate itself, different nucleotide and RNA binding modes of DEAD-box proteins may differentially increase their probability to bind to and unwind a specific duplex within a large, structured RNA.

Based on the behavior of Mss116, it has been suggested that RecA_C acts as a stationary platform for RNA binding, and unwinding is caused by the incursion of RecA_N (10). Our data on RNA binding to Hera point to the existence of an alternative model in which both RecA-like domains, connected via tight interactions with dsRNA, synergistically destabilize the dsRNA by a concerted inward incursion during closure of the helicase core upon nucleotide binding (Figure 6). A similar role of the RNA in inter-domain communication can be envisaged for (nucleotide-bound) YxiN. A synchronous movement of both domains with respect to the bound RNA may be more effective in destabilizing the RNA duplex than the inward incursion of a single domain only and might become relevant in unwinding of specific duplexes in large RNAs with complex tertiary structure.

In conclusion, the mechanism of dsRNA unwinding may be fine-tuned differently among DEAD-box helicases, probably to allow for the recognition of different RNA substrates, for different mechanisms of regulation and for the direction of DEAD-box helicases to their respective cellular targets.

SUPPLEMENTARY DATA

Supplementary Data are available at NAR Online.

ACKNOWLEDGMENTS

The authors would like to thank Ayrat Gubaev and Alexandra Andreou for helpful discussions. B.S. and D.K. conceived the research, analyzed data and wrote the manuscript. B.S. prepared materials and performed the experiments.

FUNDING

Deutsche Forschungsgemeinschaft [to D.K.].
Conflict of interest statement. None declared.

REFERENCES

1. Steimer,L. and Klostermeier,D. (2012) RNA helicases in infection and disease. *RNA Biol.*, **9**, 751–771.
2. Fairman-Williams,M.E., Guenther,U.P. and Jankowsky,E. (2010) SF1 and SF2 helicases: family matters. *Curr. Opin. Struct. Biol.*, **20**, 313–324.

3. Kossen,K., Karginov,F.V. and Uhlenbeck,O.C. (2002) The carboxy-terminal domain of the DExDH protein YxiN is sufficient to confer specificity for 23S rRNA. *J. Mol. Biol.*, **324**, 625–636.
4. Karginov,F.V., Caruthers,J.M., Hu,Y., McKay,D.B. and Uhlenbeck,O.C. (2005) YxiN is a modular protein combining a DEx(D/H) core and a specific RNA-binding domain. *J. Biol. Chem.*, **280**, 35499–35505.
5. Turner,A.M., Love,C.F., Alexander,R.W. and Jones,P.G. (2007) Mutational analysis of the Escherichia coli DEAD box protein CsdA. *J. Bacteriol.*, **189**, 2769–2776.
6. Linden,M.H., Hartmann,R.K. and Klostermeier,D. (2008) The putative RNase P motif in the DEAD box helicase Hera is dispensable for efficient interaction with RNA and helicase activity. *Nucleic Acids Res.*, **36**, 5800–5811.
7. Diges,C.M. and Uhlenbeck,O.C. (2001) Escherichia coli DbpA is an RNA helicase that requires hairpin 92 of 23S rRNA. *EMBO J.*, **20**, 5503–5512.
8. Fuller-Pace,F.V., Nicol,S.M., Reid,A.D. and Lane,D.P. (1993) DbpA: a DEAD box protein specifically activated by 23s rRNA. *EMBO J.*, **12**, 3619–3626.
9. Del Campo,M., Mohr,S., Jiang,Y., Jia,H., Jankowsky,E. and Lambowitz,A.M. (2009) Unwinding by local strand separation is critical for the function of DEAD-box proteins as RNA chaperones. *J. Mol. Biol.*, **389**, 674–693.
10. Mallam,A.L., Del Campo,M., Gilman,B., Sidote,D.J. and Lambowitz,A.M. (2012) Structural basis for RNA-duplex recognition and unwinding by the DEAD-box helicase Mss116p. *Nature*, **490**, 121–125.
11. Henn,A., Bradley,M.J. and De La Cruz,E.M. (2012) ATP utilization and RNA conformational rearrangement by DEAD-box proteins. *Annu. Rev. Biophys.*, **41**, 247–267.
12. Andreou,A.Z. and Klostermeier,D. (2012) Conformational changes of DEAD-box helicases monitored by single molecule fluorescence resonance energy transfer. *Methods Enzymol.*, **511**, 75–109.
13. Russell,R., Jarmoskaite,I. and Lambowitz,A.M. (2013) Toward a molecular understanding of RNA remodeling by DEAD-box proteins. *RNA Biol.*, **10**, 44–55.
14. Theissen,B., Karow,A.R., Kohler,J., Gubaev,A. and Klostermeier,D. (2008) Cooperative binding of ATP and RNA induces a closed conformation in a DEAD box RNA helicase. *Proc. Natl Acad. Sci. USA*, **105**, 548–553.
15. Lorsch,J.R. and Herschlag,D. (1998) The DEAD box protein eIF4A. 1. A minimal kinetic and thermodynamic framework reveals coupled binding of RNA and nucleotide. *Biochemistry*, **37**, 2180–2193.
16. Iost,I., Dreyfus,M. and Linder,P. (1999) Ded1p, a DEAD-box protein required for translation initiation in Saccharomyces cerevisiae, is an RNA helicase. *J. Biol. Chem.*, **274**, 17677–17683.
17. Banroques,J., Cordin,O., Doere,M., Linder,P. and Tanner,N.K. (2008) A conserved phenylalanine of motif IV in superfamily 2 helicases is required for cooperative, ATP-dependent binding of RNA substrates in DEAD-box proteins. *Mol. Cell Biol.*, **28**, 3359–3371.
18. Cao,W., Coman,M.M., Ding,S., Henn,A., Middleton,E.R., Bradley,M.J., Rhoades,E., Hackney,D.D., Pyle,A.M. and De La Cruz,E.M. (2011) Mechanism of Mss116 ATPase reveals functional diversity of DEAD-box proteins. *J. Mol. Biol.*, **409**, 399–414.
19. Henn,A., Medalia,O., Shi,S.P., Steinberg,M., Franceschi,F. and Sagi,I. (2001) Visualization of unwinding activity of duplex RNA by DbpA, a DEAD box helicase, at single-molecule resolution by atomic force microscopy. *Proc. Natl. Acad. Sci. USA*, **98**, 5007–5012.
20. Sengoku,T., Nureki,O., Nakamura,A., Kobayashi,S. and Yokoyama,S. (2006) Structural basis for RNA unwinding by the DEAD-box protein Drosophila Vasa. *Cell*, **125**, 287–300.
21. Hilbert,M., Karow,A.R. and Klostermeier,D. (2009) The mechanism of ATP-dependent RNA unwinding by DEAD box proteins. *Biol. Chem.*, **390**, 1237–1250.
22. Del Campo,M. and Lambowitz,A.M. (2009) Structure of the Yeast DEAD box protein Mss116p reveals two wedges that crimp RNA. *Mol. Cell*, **35**, 598–609.
23. Henn,A., Cao,W., Hackney,D.D. and De La Cruz,E.M. (2008) The ATPase cycle mechanism of the DEAD-box rRNA helicase, DbpA. *J. Mol. Biol.*, **377**, 193–205.
24. Chen,Y., Potratz,J.P., Tijerina,P., Del Campo,M., Lambowitz,A.M. and Russell,R. (2008) DEAD-box proteins can completely separate an RNA duplex using a single ATP. *Proc. Natl. Acad. Sci. USA*, **105**, 20203–20208.
25. Liu,F., Putnam,A. and Jankowsky,E. (2008) ATP hydrolysis is required for DEAD-box protein recycling but not for duplex unwinding. *Proc. Natl. Acad. Sci. USA*, **105**, 20209–20214.
26. Hilbert,M., Kebbel,F., Gubaev,A. and Klostermeier,D. (2011) eIF4G stimulates the activity of the DEAD box protein eIF4A by a conformational guidance mechanism. *Nucleic Acids Res.*, **39**, 2260–2270.
27. Aregger,R. and Klostermeier,D. (2009) The DEAD box helicase YxiN maintains a closed conformation during ATP hydrolysis. *Biochemistry*, **48**, 10679–10681.
28. Harms,U., Andreou,A.Z., Gubaev,A. and Klostermeier,D. (2014) eIF4B, eIF4G and RNA regulate eIF4A activity in translation initiation by modulating the eIF4A conformational cycle. *Nucleic Acids Res.*, **42**, 7911–7922.
29. Morlang,S., Weglohner,W. and Franceschi,F. (1999) Hera from Thermus thermophilus: the first thermostable DEAD-box helicase with an RNase P protein motif. *J. Mol. Biol.*, **294**, 795–805.
30. Klostermeier,D. (2013) Rearranging RNA structures at 75 degrees C? towards the molecular mechanism and physiological function of the Thermus thermophilus DEAD-box helicase hera. *Biopolymers*. **99** , 1137–1146
31. Studier,F.W. (2005) Protein production by auto-induction in high density shaking cultures. *Protein Expr. Purif.*, **41**, 207–234.
32. Karow,A.R., Theissen,B. and Klostermeier,D. (2007) Authentic interdomain communication in an RNA helicase reconstituted by expressed protein ligation of two helicase domains. *FEBS J.*, **274**, 463–473.
33. Rudolph,M.G., Heissmann,R., Wittmann,J.G. and Klostermeier,D. (2006) Crystal structure and nucleotide binding of the Thermus thermophilus RNA helicase Hera N-terminal domain. *J. Mol. Biol.*, **361**, 731–743.
34. Rudolph,M.G., Wittmann,J.G. and Klostermeier,D. (2009) Crystallization and preliminary characterization of the Thermus thermophilus RNA helicase Hera C-terminal domain. *Acta Crystallogr. Sect. F. Struct. Biol. Cryst. Commun.*, **65**, 248–252.
35. Klostermeier,D. (2013) Rearranging RNA structures at 75 degrees C? toward the molecular mechanism and physiological function of the thermus thermophilus DEAD-box helicase hera. *Biopolymers*, **99**, 1137–1146.
36. Caruthers,J.M., Hu,Y. and McKay,D.B. (2006) Structure of the second domain of the Bacillus subtilis DEAD-box RNA helicase YxiN. *Acta Crystallogr. Sect. F. Struct. Biol. Cryst. Commun.*, **62**, 1191–1195.
37. Gill,S.C. and von Hippel,P.H. (1989) Calculation of protein extinction coefficients from amino acid sequence data. *Anal. Biochem.*, **182**, 319–326.
38. Feinstein,E., Deikus,G., Rusinova,E., Rachofsky,E.L., Ross,J.B. and Laws,W.R. (2003) Constrained analysis of fluorescence anisotropy decay: application to experimental protein dynamics. *Biophys. J.*, **84**, 599–611.
39. Fiserova,E. and Kubala,M. (2012) Mean fluorescence lifetime and its error. *J. Lumin.*, **132**, 2059–2064.
40. Weinreis,S.A., Ellis,J.P. and Cavagnero,S. (2010) Dynamic fluorescence depolarization: a powerful tool to explore protein folding on the ribosome. *Methods*, **52**, 57–73.
41. Lakowicz,J.R. (2006) *Principles of Fluorescence Spectroscopy*. 3rd ed. Springer, New York.
42. Deprez,E., Tauc,P., Leh,H., Mouscadet,J.F., Auclair,C., Hawkins,M.E. and Brochon,J.C. (2001) DNA binding induces dissociation of the multimeric form of HIV-1 integrase: a time-resolved fluorescence anisotropy study. *Proc. Natl. Acad. Sci. USA*, **98**, 10090–10095.
43. Bialik,C.N., Wolf,B., Rachofsky,E.L., Ross,J.B. and Laws,W.R. (1998) Dynamics of biomolecules: assignment of local motions by fluorescence anisotropy decay. *Biophys. J.*, **75**, 2564–2573.
44. Chuang,T.J. and Eisenthal,K.B.. (1972) Theory of fluorescence depolarization by anisotropic rotational diffusion. *J. Chem. Phys.*, **57**, 5094–5097.
45. Ferguson,B.Q. and Yang,D.C. (1986) Methionyl-tRNA synthetase induced 3′-terminal and delocalized conformational transition in tRNAfMet: steady-state fluorescence of tRNA with a single fluorophore. *Biochemistry*, **25**, 529–539.

46. Cordin,O., Banroques,J., Tanner,N.K. and Linder,P. (2006) The DEAD-box protein family of RNA helicases. *Gene*, **367**, 17–37.
47. Bleichert,F. and Baserga,S.J. (2007) The long unwinding road of RNA helicases. *Mol. Cell*, **27**, 339–352.
48. Andersen,C.B., Ballut,L., Johansen,J.S., Chamieh,H., Nielsen,K.H., Oliveira,C.L., Pedersen,J.S., Seraphin,B., Le Hir,H. and Andersen,G.R. (2006) Structure of the exon junction core complex with a trapped DEAD-box ATPase bound to RNA. *Science*, **313**, 1968–1972.
49. Caruthers,J.M., Johnson,E.R. and McKay,D.B. (2000) Crystal structure of yeast initiation factor 4A, a DEAD-box RNA helicase. *Proc. Natl. Acad. Sci. USA*, **97**, 13080–13085.
50. Pause,A., Methot,N. and Sonenberg,N. (1993) The HRIGRXXR region of the Dead box RNA helicase eukaryotic translation initiation factor-4a is required for RNA-binding and ATP hydrolysis. *Mol. Cell. Biol.*, **13**, 6789–6798.
51. Polach,K.J. and Uhlenbeck,O.C. (2002) Cooperative binding of ATP and RNA substrates to the DEAD/H protein DbpA. *Biochemistry*, **41**, 3693–3702.
52. Mallam,A.L., Del Campo,M., Gilman,B., Sidote,D.J. and Lambowitz,A.M. (2012) Structural basis for RNA-duplex recognition and unwinding by the DEAD-box helicase Mss116p. *Nature*, **490**, 121–125.
53. Mallam,A.L., Jarmoskaite,I., Tijerina,P., Del Campo,M., Seifert,S., Guo,L., Russell,R. and Lambowitz,A.M. (2011) Solution structures of DEAD-box RNA chaperones reveal conformational changes and nucleic acid tethering by a basic tail. *Proc. Natl. Acad. Sci. USA*, **108**, 12254–12259.
54. Theissen,B., Karow,A.R., Kohler,J., Gubaev,A. and Klostermeier,D. (2008) Cooperative binding of ATP and RNA induces a closed conformation in a DEAD box RNA helicase. *Proc. Natl. Acad. Sci. USA*, **105**, 548–553.
55. Rajagopal,V., Park,E.H., Hinnebusch,A.G. and Lorsch,J.R. (2012) Specific domains in yeast translation initiation factor eIF4G strongly bias RNA unwinding activity of the eIF4F complex toward duplexes with 5′-overhangs. *J. Biol. Chem.*, **287**, 20301–20312.
56. Kaminker,I., Sushenko,A., Potapov,A., Daube,S., Akabayov,B., Sagi,I. and Goldfarb,D. (2011) Probing conformational variations at the ATPase site of the RNA helicase DbpA by high-field electron-nuclear double resonance spectroscopy. *J. Am. Chem. Soc.*, **133**, 15514–15523.
57. Jarmoskaite,I., Bhaskarann,H., Seifert,S. and Russell,R. (2014) DEAD-box protein Cyt-19 is activated by exposed helicase in group I intron RNA. *Proc. Natl. Acad. Sci. USA*, **111**, E2928–E2936 .